International Journal of Nanomedicine

Dovepress
Taylor & Francis Group

Open Access Full Text Article

ORIGINAL RESEARCH

A Cell Membrane-Coated Gold Nanoparticle-Based Drug Delivery System for Enhanced Antitumor Therapy in Breast Cancer

Haiguang Zhang[1], Junchuang Liu[2], Yinli Wang[2], Aiqin Cai[3], Yitian Tang[4], Jinjin Zhao[4], Hongchang Yuan[2]

[1]Department of Gynaecology and Obstetrics, The First Affiliated Hospital of Xinxiang Medical University, Xinxiang, Henan Province, People's Republic of China; [2]Department of Clinical Pharmacy, The First Affiliated Hospital of Xinxiang Medical University, Xinxiang, Henan Province, People's Republic of China; [3]Department of Infection Management, The First Affiliated Hospital of Xinxiang Medical University, Xinxiang, Henan Province, People's Republic of China; [4]Department of Clinical Lab, The First Affiliated Hospital of Xinxiang Medical University, Xinxiang, Henan Province, People's Republic of China

Correspondence: Jinjin Zhao; Hongchang Yuan, Email hdzhaojinjin@163.com; 116597551@qq.com

Purpose: Doxorubicin (DOX) is a first-line chemotherapeutic agent widely recognized for its efficacy in inhibiting tumor growth. However, its clinical utility is limited by systemic toxicity, adverse side effects, and the emergence of multidrug resistance. To address these challenges, we developed a cell membrane-coated nanodrug delivery system in which DOX is loaded onto gold nanoparticles (AuNPs) via electrostatic adsorption, with the cell membrane acted as a biomimetic targeting component to improve therapeutic outcomes and reduce off-target toxicity.

Methods: The successful construction of M@DOX@AuNPs was confirmed by UV-Vis absorption spectroscopy and transmission electron microscope. Antitumor effects were evaluated through both in vitro and in vivo experiments. Biological safety was evaluated via histopathological staining and blood biochemical analysis.

Results: M@DOX@AuNPs demonstrated favorable physical stability and exhibited time-dependent drug release profiles. Cellular uptake studies revealed that M@DOX@AuNPs were internalized more efficiently in 4T1 and MDA-MB-231 cells compared to free DOX or DOX@AuNPs. Moreover, M@DOX@AuNPs significantly inhibited tumor cell viability and induced apoptosis in vitro, whereas free AuNPs or cell membranes alone showed no detrimental effects on tumor cell viability. In a mouse tumor model, M@DOX@AuNPs exhibited pronounced anti-tumor efficacy without inducing structure damage to major organs or causing significant alterations in blood cell counts and serum biochemical markers.

Conclusion: These findings indicate that M@DOX@AuNPs represent a promising targeted chemotherapeutic agent for improved tumor therapy.

Keywords: doxorubicin, gold nanoparticles, cell membrane, nano-drug delivery system, tumor therapy

Introduction

Breast cancer poses a significant threat to women's health, resulting in 665,684 deaths worldwide in 2022.[1] Current treatment modalities for breast cancer include chemotherapy,[2] radiotherapy,[3] hormone therapy,[4] immunotherapy[5] and targeted therapy.[6] The treatment of triple-negative breast cancer (TNBC) is particularly challenging due to the lack of expression of estrogen receptor (ER), progesterone receptor (PR) and human epidermal growth factor receptor (HER2).[7] Doxorubicin, as a first-line chemotherapeutic agent, is widely utilized in clinical practice.[8] However, the systemic toxicity, adverse side effects, and development of multidrug resistance associated with conventional chemotherapy underscore the necessitate for innovative therapeutic alternatives.[9,10]

The Nanoparticle drug delivery system has emerged as a promising approach for tumor management.[11] Nanotechnology holds significant potential for enhancing diagnostic accuracy and addressing therapeutic challenges

Received: 7 August 2025
Accepted: 14 December 2025
Published: 22 December 2025

associated with current treatment modalities.[12,13] Owing to their unique physical and chemical properties, nanoparticle-based delivery systems can enhance the efficacy of tumor treatments.[14] Several nanoparticle-based drugs have previously received approval from the US Food and Drug Administration (FDA) for targeted cancer therapy.[15] The most commonly used nanocarrier systems include lipid-based nanoparticles,[16] polymeric nanoparticles,[17] inorganic based nanoparticles[18] and metallic based nanoparticles.[19]

Due to their unique physicochemical properties and broad applicability in biomedical fields, gold nanoparticles (AuNPs) have the potential to improve the specificity, efficacy, and safety of cancer treatment while minimizing systemic toxicity and addressing drug resistance.[20,21] AuNPs typically range in size from 1 to 100 nm.[22] Since tumor blood vessels are irregular, disorganized, and exhibit larger gaps between endothelial cells, nanoparticles within the size range of 10–200 nm can more effectively penetrate and accumulate in tumor tissues, a phenomenon known as the enhanced permeation and retention effect (EPR).[23]

Due to the heterogeneity of cancer cells and the complexity of the tumor microenvironment (TME), AuNPs exhibit limited specificity towards cancer cells, even when functionalized with targeting agents such as antibodies or peptides.[24] Furthermore, AuNPs may elicit immune response that compromise their therapeutic efficacy, as they are often recognized by the immune system as foreign entities.[24] To address these limitations, cell membrane-based coatings have emerged as a promising alternative.[17,25] Nature cell membranes possess a complex protein composition and support various biological functions, such as immune evasion, precise antigen presentation, and cell- or tissue-specific targeting capabilities.[26] Cell membrane coatings can be effectively derived from multiple cell types, including erythrocytes,[27,28] platelets,[29] macrophages,[30] cancer cells,[31] stem cells[32] and even bacteria.[33] Among these, Cancer cell membranes, owing to their inherent abilities for immune escape and tumor-specific targeting abilities, are increasingly being utilized in anticancer drug delivery systems.[34]

In this study, two triple-negative breast cancer cell lines - 4T1 and MDA-MB-231 - were employed as tumor models. The 4T1 cell line demonstrates growth and metastatic features closely resembling those of human breast cancer.[35] The MDA-MB-231 cell line, which exhibits epithelioid morphology and was derived from a metastatic pleural effusion sample of a 51-year-old White female with adenocarcinoma of the breast, is widely utilized as a transfection host in breast cancer research.[36] Electrostatic adsorption was employed to construct a drug delivery system (DOX@AuNPS), wherein AuNPs carried a negative charge while DOX was positively charged. Subsequently, tumor cell membranes were coated onto DOX@AuNPs through ultrasonication of the mixture, resulting in the successful fabrication of a cell membrane-coated drug delivery system (M@DOX@AuNPs). Hemolysis assays confirmed the biocompatibility of M@DOX@AuNPs, and phagocytosis experiments verified their targeting capability. Furthermore, MTT assays and flow cytometry analyses demonstrated effective in vitro tumor inhibition, while animal studies exhibited excellent anti-tumor efficacy in a mouse tumor model. Histopathological evaluation via H&E staining, along with blood cell counts and serum biochemistry analyses, confirmed the biological safety of the treatment. By synergistically integrating these innovations, this study offers novel insights and advancements that may contribute to the development of more effective therapeutic strategies for breast tumor, and addressing critical challenges in the current treatment paradigms.

Materials and Method

Materials

Tetrachloroauric (III) acid trihydrate ($HAuCl_4•3H_2O$), Sodium citrate, 1-(4,5-dimethylpyridin-2-yl-3,5-diphenylformamide (MTT) and were purchased from Sigma Aldrich Co., Ltd. (Shanghai, China). Doxorubicin hydrochloride was purchased from MedChemExpress Co., Ltd. (Shanghai, China). Fetal bovine serum (FBS), Roswell Park Memorial Institute 1640 (RPMI-1640) medium, and Dulbecco's Modified Eagle's medium (DMEM) were got from Corring Co., Ltd. (Manassas, USA). DAPI staining Solution and Nuclear and Cytoplasmic Protein Extraction Kit were obtained from Beyotime Co., Ltd. (Jiangsu, China). All other reagents were analytical grade and provided by Macklin Co., Ltd. (Shanghai, China).

Instrumentation

The UV-visible absorbance spectra were obtained employing the SHIMADZU LabSolutions UV model UV2600s spectrophotometer (Shimadzu Corporation, Japan). The size and zeta potential of nanoparticles were acquired using a dynamic light scattering (DLS) instrument, Mastersizer 3000 Ultra (Spectrisplc, France). Transmission electron microscopy (TEM) images were acquired using a JEOL JEM-F200 microscope (JEOL Ltd., Japan). MTT assay absorbance values were recorded using a Multiskan Sky Microplate Spectrophotomerer (BioTek Instruments. Inc. USA).

Synthesis of AuNPs

The synthesis of AuNPs was conducted based on our previously reported method with minor modification.[37] In brief, 0.5 mL of $HAuCl_4$ solution (1%) was dissolved in ultrapure water (50mL) in a round-bottomed flask under continuous stirring. The mixture was heated to 95 °C, followed by the rapid addition of 1.25 mL Sodium citrate solution (1%). The reaction was maintained for 15 min until the solution color changed from faint yellow to wine red. After additional 15 min of stirring, the resulting product was cooled down to room temperature and stored at 4 °C for future use.

Synthesis of M@DOX@AuNPs

Tumor cell membrane (M) was collected using a Nuclear and Cytoplasmic Protein Extraction Kit.[38] Briefly, cells in the logarithmic growth phase were washed with PBS, scraped from the culture dish, and resuspended in 200 μL of cytoplasmic protein extraction reagent A. The cells were then thoroughly dispersed through vigorous vertexing. Subsequently, 10 μL of regent B was added to lyse the cells. Following centrifugation at 16,000g for 5min, the cell membrane pellet was collected from the bottom of the centrifuge tube.

SDS-PAGE and Western blot were performed to detect acquired cell membranes. Cell lysates or membrane fractions were mixed with loading buffer and boiled for 5 minutes. A total of 20ng of protein was loaded per lane for SDS-PAGE. The gel was stained with Coomassie Brilliant Blue R250 (10mg/mL), destained with 50% methanol, and subsequently photographed. For CD47 detection, following SDS-PAGE, proteins on the gel were transferred onto a PVDF membrane, blocked with 5% skim milk, incubated with primary anti-CD47 antibody, and then probed with HRP-conjugated secondary antibody. Protein bands were visualized using enhanced chemiluminescence (ECL) detection reagent.

DOX was loaded onto AuNPs through electrostatic adsorption. Briefly, 5mL of DOX solution (1mg/mL) was added to 5 mL of AuNPs solution (1mg/mL), followed by stirring at 25 °C for 4 hours to form DOX-loaded AuNPs (DOX@AuNPs). To coat the cell membrane onto DOX@AuNPs, the membrane isolated from 1×10^7 cells was mixed with the obtained DOX@AuNPs and subjected to ultrasonication at 100% amplitude for 30 mins under ice-cooling conditions. Finally, the mixture was centrifuged to collect the cell membrane-coated nanoparticles M@DOX@AuNPs.

Quantification of DOX on M@DOX@AuNPs

The drug conjugated to AuNPs was measured using UV-visible absorbance spectroscopy. The standard cure was generated by measuring the absorbance of known concentrations of DOX. After DOX mixed with AuNPs for 4 hours, the producer was centrifuged and recorded the absorbance of the supernatant which corresponds to that of unbound DOX. Drug loaded on AuNPs was calculated by the concentration difference of DOX before and after the reaction.

Drug Release Analysis

To establish the time-responsive drug release mechanism, an in vitro drug release analysis was conducted using UV-visible absorbance spectroscopy. The prepared M@DOX@AuNPs and DOX@AuNPs were separately resuspended in citrate buffer (pH 6.5) or PBS buffer (pH 7.4) for comparative analysis. At predetermined time intervals, aliquots of the supernatant were collected for UV-visible spectroscopic analysis, and the drug release profile was subsequently evaluated as follows:

$$\text{Drug release} = (\text{Drug}_{\text{time point}}/\ \text{Drug}_{\text{initial}}) \times 100$$

 https://doi.org/10.2147/IJN.S559080

Hemolysis Test

Red blood cells were collected from BABL/c mice via centrifugation. Following washing with phosphate-buffered saline (PBS), the red blood cells were resuspended in M@DOX@AuNPs solutions at varying concentrations. Ultrapure water and 0.9% NaCl solution were employed as positive and negative controls, respectively. After incubation for 12 hours, the supernatant was analyzed by UV-visible absorbance spectroscopy. Hemolysis was assessed using the following calculation formula:

$$\text{Hemolysis} = (A_{\text{test group}} / A_{\text{positive control}}) \times 100$$

In vitro Material Uptake

The cell lines used in this study, including 4T1 and MDA-MB-231, were all obtained from National Collection of Authenticated Cell Cultures (Shanghai, China). Cells (4T1 and MDA-MB-231) in the logarithmic growth phase were seeded into 6-well plates. Following overnight culture, the cells were incubated with DOX, DOX@AuNPs, or M@DOX@AuNPs in the CO_2 incubator for 8 hours. Subsequently, the cells were washed with PBS and fixed with glutaraldehyde, followed by treatment with DIPA for nuclear staining. Fluorescence intensity across different cell samples was captured using a laser confocal microscope. Additionally, flow cytometry was employed for semi-quantitative analysis of drug uptake by tumor cells after incubation with various nanoparticles for 8 hours.

In vitro Cytotoxicity Analysis

Cells (4T1 and MDA-MB-231) were seeded in 96-well plates at a density of 0.8×10^4 cells per well. Following overnight culture, the cells were treated with AuNPs, Cell membrane, DOX, DOX@AuNPs, or M@DOX@AuNPs at different concentrations for 24 hours, with PBS-treated cells serving as the control group. Cell viability was measured using the MTT assay according to previously established protocols. Following measurement of the absorbance of each well, cell viability was calculated using the following formula:

$$\text{Cell viability} = (A_{\text{treated}} / A_{\text{control}}) \times 100$$

IC50 values for DOX, DOX@AuNPs, and M@DOX@AuNPs against 4T1 and MDA-MB-231 cells were determined using GraphPad Prism (10.4.2) software by analyzing cell viability across various concentrations.

For detection of cell apoptosis, cells were harvested and washed with staining buffer after treatment with different drugs for 24 hours. Subsequently, the cells were incubated with Annexin V-APC for 15mins, followed by the addition of 7-AAD for additional 5 mins. Apoptotic cells across different groups were then analyzed using flow cytometry.

Blood Biochemistry Analysis and H&E Staining

Twenty-four mice were randomly assigned to four groups and administered intravenous injections of PBS, DOX, DOX@AuNPs, or M@DOX@AuNPs on 5 occasions, with a one-day interval between each injection. Two days after the final injection, Whole blood samples were collected from the mice, following which the animals were euthanized to allow for the collection of hearts, livers, spleens, lungs and kidneys. The collected blood samples were first subjected to routine blood analysis, then centrifuged to separate the serum. Serum levels of alanine aminotransferase (ALT), aspartate aminotransferase (AST) and Creatinine were subsequently measured.[39] The excised organs were fixed in formaldehyde and embedded in paraffin wax; tissue sectioning, staining, and scanning were performed by Servicebio Co., Ltd. (Wuhan, China).

In vivo Antitumor Efficacy

The experimental steps to establish the 4T1 mouse melanoma model followed the protocol approved by Xinxiang Medical University (number of ethical permissions: EC-023-036) and the Guide for the Care and Use of Laboratory Animals (Washington (DC): National Academies Press (US); 2011). 4T1 cells in the logarithmic growth phase were suspended in PBS at a concentration of 1×10^7cells per mL. To establish the tumor model, 100 μL of the cell suspension was injected subcutaneously into the right flank of BABL/C mice (6–8 weeks purchased from Vital River Co., Ltd.

Beijing, China). 4 days later, when the tumors became palpable, the mice were randomly divided into four groups (6 mice in each group) and administered intravenous injections of PBS, DOX (5 mg/Kg), DOX@AuNPs (5 mg/Kg, based on the DOX content), or M@DOX@AuNPs (5 mg/Kg, based on the DOX content) 5 times with a one-day interval between each injection. Tumor size was measured every two days using a vernier caliper, and body weight was recorded simultaneously. Following the treatment period, the mice were euthanized, and the tumors were excised, weighed, and photographed. Tumor volumes (V) were calculated using the following formula:

$$V = \text{Tumor length} \times \text{Tumor width}^2/2$$

For the in vivo biodistribution study, mice were euthanized 8 hours after the initial administration of PBS, DOX, DOX@AuNPs, or M@DOX@AuNPs. Major organs and tumor tissues were then harvested, and fluorescent images were acquired using the LumiFluor AniView100 imaging system (Guangzhou Biolight Biotechnology Co., Ltd).

Statistical Analysis

All experiments were conducted at least 3 times ($n \geq 3$ for cell experiments and $n \geq 6$ for mouse experiments), with results presented as mean ± standard deviation (SD). Statistical analysis was performed using one-way analysis of variance (ANOVA) followed by an unpaired two-tailed Student's *t*-test,[40] utilizing GraphPad Prism software (GraphPad Software, Inc., CA, USA). Levels of statistical significance were defined as follows: ns (not significant), * $P < 0.05$, **P < 0.01, *** $P < 0.005$, **** $P < 0.001$.

Results and Discussion

Characterization of M@DOX@AuNPs

The isolated cell membranes were analyzed by SDS-PAGE and Western Blot, as shown in Figure S1, compared with the total protein in cell lysates, the protein in cell membrane was less, and the CD47 protein was enriched in the cell membrane.

The size of different nanoparticles was presented in Figure 1A. As reported in previous studies, the particle size of AuNPs was approximately 20 nm, and the particle size increased with the sequential loading of DOX and cell membrane.

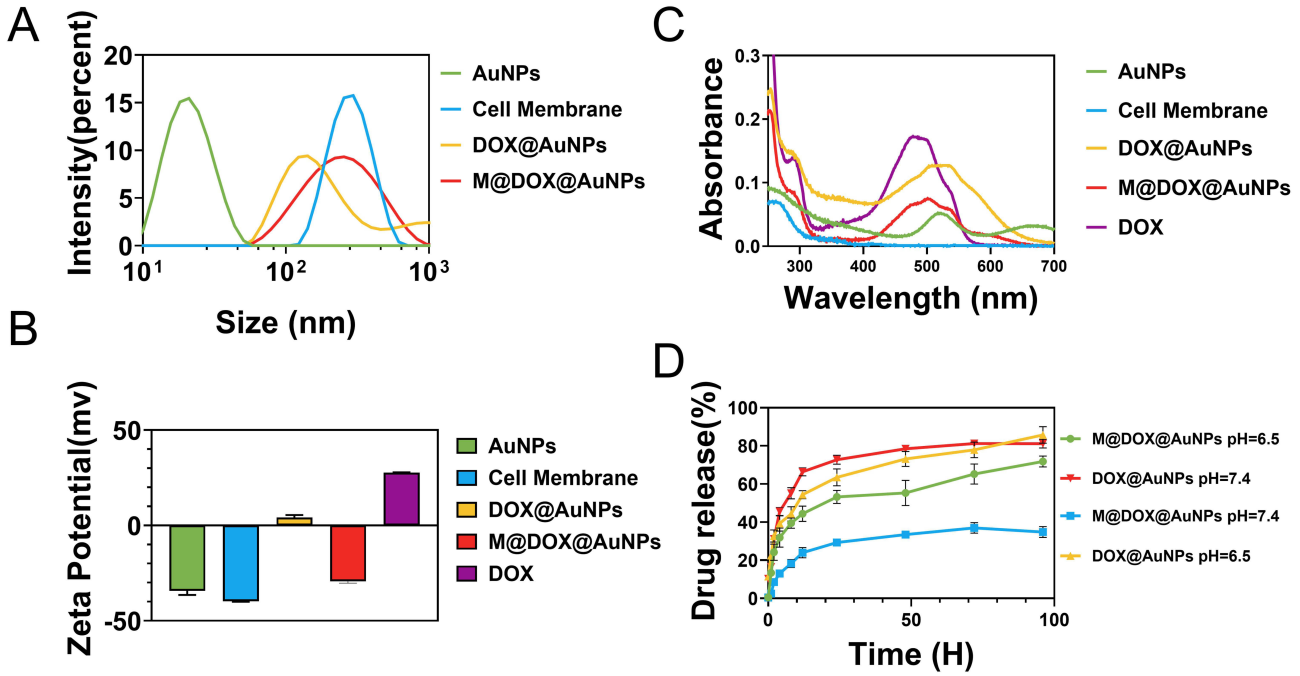

Figure 1 (**A**) Size distribution, (**B**) UV-vis absorbance, and (**C**) Zeta potential of AuNPs, Cell membrane, DOX, DOX@AuNPs, and M@DOX@AuNPs. (**D**) Drug release profiles of DOX@AuNPs and M@DOX@AuNPs in PBS (pH 7.4) and citrate buffer solution (pH 6.5).

https://doi.org/10.2147/IJN.S559080

The Zeta potential also varied during the assembly of the drug delivery system. The Zeta potentials of the synthesized AuNPs and free DOX were measured to be approximately −34.30 ± 2.15 mV and 27.70 ± 0.17 mV, respectively (Figure 1B). DOX@AuNPs, with a Zeta potential of about 4.16 ± 1.34 mV, were formed through electrostatic interaction between DOX and AuNPs. Subsequently, cell membrane, which exhibited a Zeta potential of approximately −39.77 ± 0.31 mV, was coated onto the DOX@AuNPs, resulting in nanoparticles with a final zeta potential of −29.27 ± 1.06 mV. The successful construction of the drug delivery system was further confirmed by UV-Vis spectroscopy. As shown in Figure 1C, consistent with previous reports, the absorbance peaks at 520nm and 490nm correspond to AuNPs and DOX, respectively. The broadened absorbance peak at around 550nm for DOX@AuNPs indicates that DOX was effectively conjugated onto the surface of AuNPs. Based on the calculations, it was determined that 1mg of AuNPs can load 210 μg of DOX. For the cell membrane, the characteristic absorbance peak appeared at 280nm and this same peak was observed in M@DOX@AuNPs after the cell membrane coating process.

Before the application of M@DOX@AuNPs in tumor treatment, their DOX release profiles were evaluated in citrate buffer (pH 6.5), which mimics the tumor microenvironment, and in PBS buffer (pH 7.4), simulating physiological conditions in the bloodstream. As shown in Figure 1D, DOX was rapidly released from DOX@AuNPs within the first 10 hours under both pH conditions, followed by a sustained release phase. In contrast, M@DOX@AuNPs exhibited significantly reduced drug release at pH 7.4, with less than 40% of DOX released after 96 hours, whereas approximately 80% of the drug was released at pH 6,5 under the same time frame. These results indicate that cell membrane coating effectively minimizes non-specific drug release while enabling enhanced release under acidic conditions resembling the tumor microenvironment.

The morphology of AuNPs and M@DOX@AuNPs is presented in Figure 2, AuNPs exhibit a uniform spherical structure with a diameter of approximately 20 nm (Figure 2A and B). Following the coating with cell membrane, a distinct thin layer was presented on the surface of AuNPs (Figure 2C and D). Energy Dispersive Spectroscopy (EDS) analysis of M@DOX@AuNPs is presented in Figure S2, showing the presence of key elements in biofilms, including C, N, P and S. These observations indicate that DOX was successfully loaded onto the AuNPs, and that the cell membrane was effectively coated.

In vitro Biosafety of M@DOX@AuNPs

To ensure clinical safety, a hemolysis assay was performed to evaluate the blood compatibility of M@DOX@AuNPs. The results are presented in Figure S3, 4 hours after co-incubation with M@DOX@AuNPs at various concentrations (12.5, 25, 50, 100, 200 μg/mL), the supernatants remained nearly transparent (Figure S3A), and the calculated hemolysis rates were below 5% (Figure S3B).

Evaluation of Phagocytosis of Tumor Cells

The phagocytosis of drugs by tumor cells was the initial step in achieving their full therapeutic effect. DOX is capable of emitting red fluorescence under a fluorescence microscope, and DIPA was used to label the cell nucleus. As demonstrated by the CLSM results, after an 8-hour incubation with DOX, red fluorescence was observed within the tumor cells. With the assistance of AuNPs, the intensity of red fluorescence in the DOX@AuNPs treated tumor cells increased significantly. Upon coating the cell membrane, M@DOX@AuNPs exhibited the strongest and most widely distributed red fluorescence within the tumor cells (Figure 3A and B). These findings were corroborated by flow cytometry results (Figure S4), which aligned with the CLSM observations as shown in Figure 3A and B. Collectively, these results suggested that M@DOX@AuNPs hold significant potential as a nanoparticle-based drug delivery system for tumor therapy.

In vitro Cytotoxicity Studies

To evaluate the anti-tumor efficacy of the drug delivery system, the cell viability of tumor cells (4T1 and MDA-MB-231) was first assessed using the MTT assay after exposure to varying concentrations of AuNPs or cell membrane for 24 hours. As presented in Figure 4, neither AuNPs nor the cell membrane exhibited a significant effect on the viability of 4T1 or MDA-MB-231 cells.

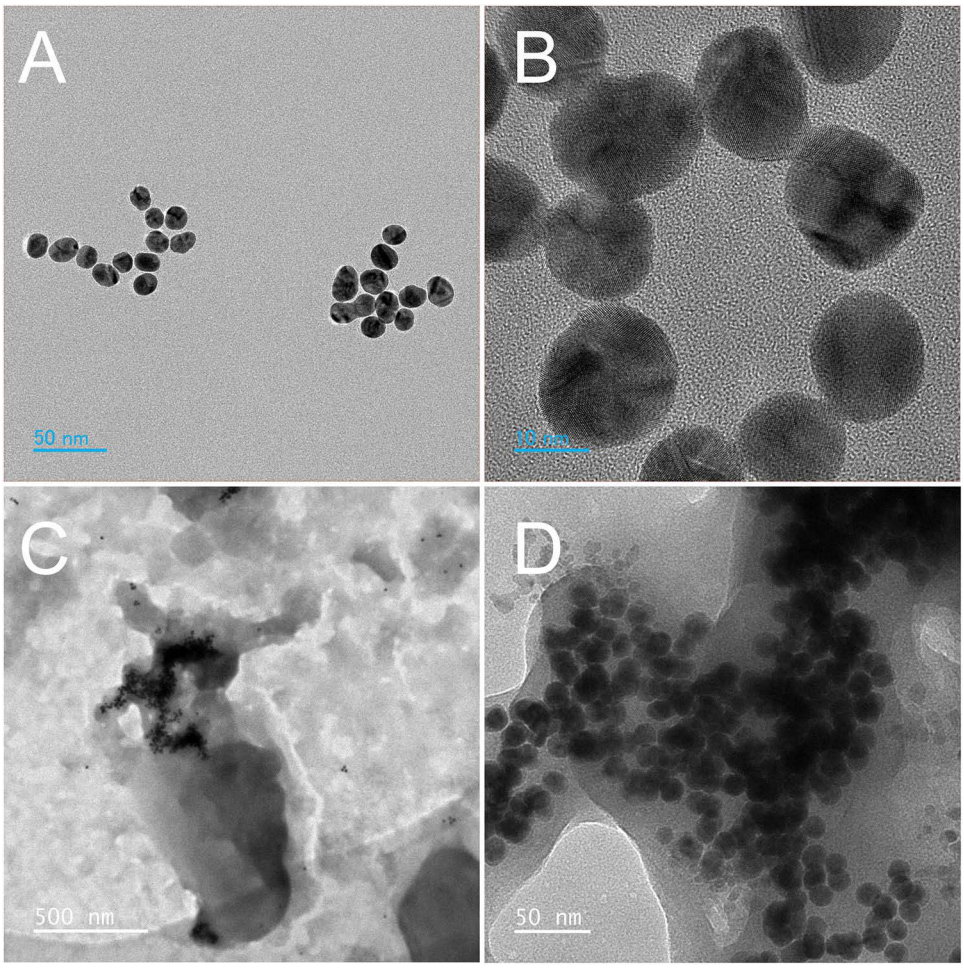

Figure 2 TEM images of (**A** and **B**) AuNPs and (**C** and **D**) M@DOX@AuNPs.

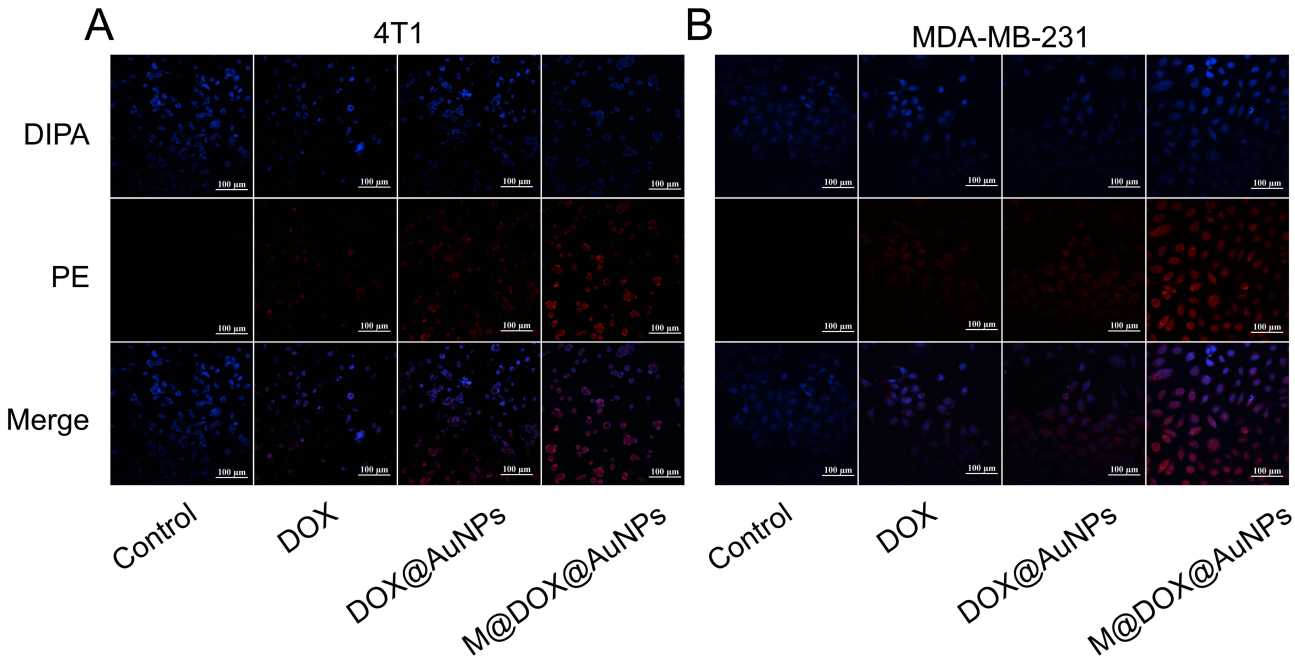

Figure 3 Confocal microscopy images showing the nuclear staining of (**A**) 4T1 cells and (**B**) MDA-MB-231 cells with DIPA for PBS, DOX, DOX@AuNPs and M@DOX@AuNPs.

https://doi.org/10.2147/IJN.S559080

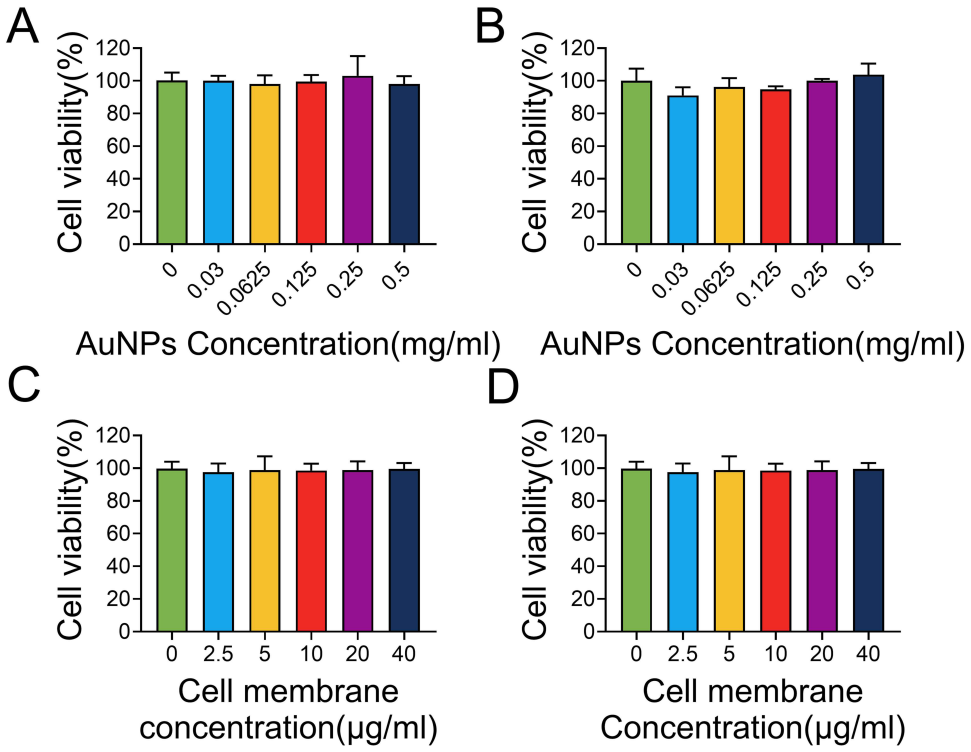

Figure 4 Cell viability of (**A** and **C**) 4T1 cells and (**B** and **D**) MDA-MB-231 cells treated with different concentrations of (**A** and **B**) AuNPs, or (**C** and **D**) cell membrane.

Subsequently, the cytotoxic effects of DOX, DOX@AuNPs and M@DOX@AuNPs on 4T1 and MDA-MB-231 cells were examined (Figure 5A and B). Notably, M@DOX@AuNPs displayed significantly enhanced cytotoxicity against cancer cells compared to DOX and DOX@AuNPs across different concentrations. Meanwhile, the IC 50 values of DOX, DOX@AuNPs and M@DOX@AuNPs against 4T1 and MDA-MB-231 cells are presented in Figure S5, indicating a significant reduction in IC50 upon loading of the drug onto AuNPs, with a further decrease observed when the nanoparticles were coated with cell membrane. Given that neither AuNPs nor the cell membrane alone affected tumor

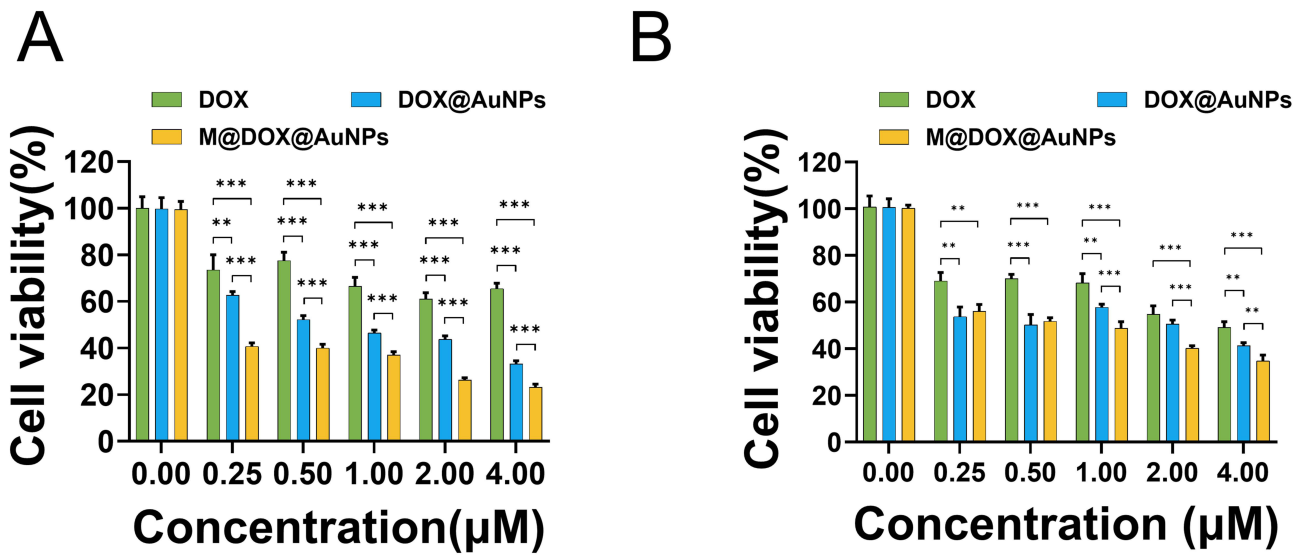

Figure 5 Cell viability of (**A**) 4T1 cells and (**B**) MDA-MB-231 cells treated with different concentrations of DOX, DOX@AuNPs, or M@DOX@AuNPs. Data represent the mean ± SEM from three repeats. Statistical significance among groups: **P < 0.01, ***P < 0.005.

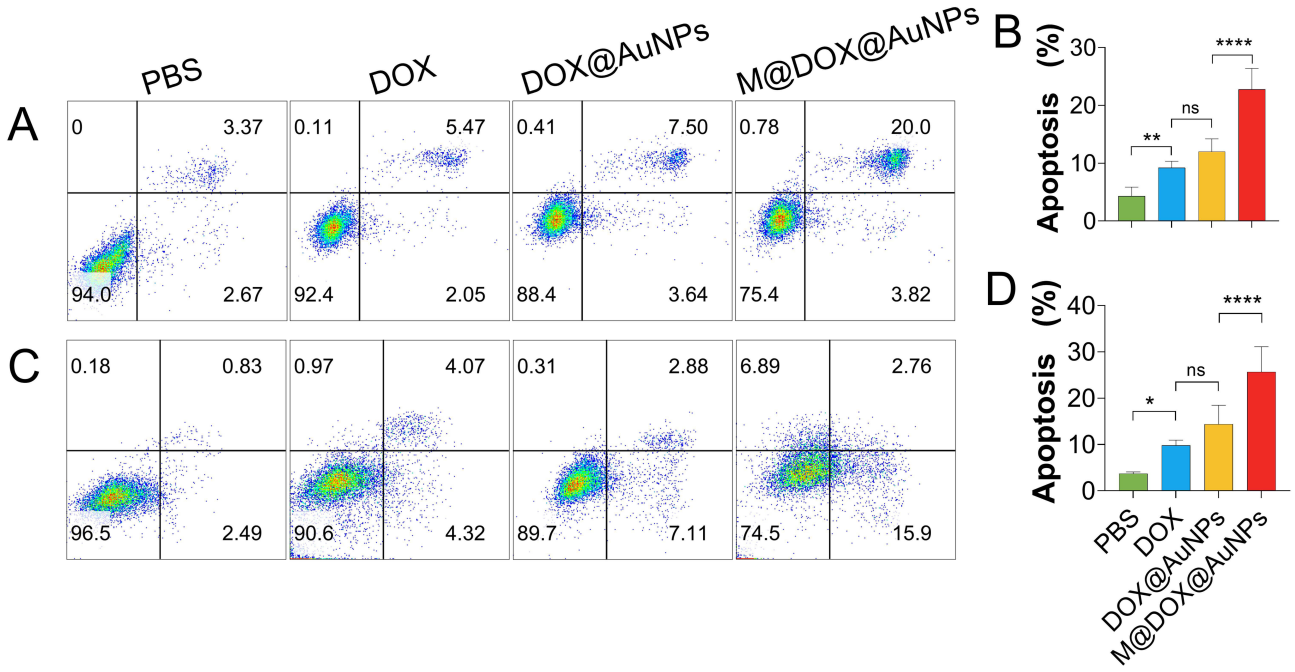

Figure 6 Cell apoptosis in (A) 4T1 cells and (C) MDA-MB-231 following treatment with various agents. Statistical analysis of the apoptosis ratio in (B) 4T1 cells and (D) MDA-MB-231 cells treated with different compounds. Data represent the mean ± SEM from three repeats. Statistical significance among groups: not significant (ns), *P < 0.05, **P < 0.01, ****P < 0.001.

cell viability, the observed differences may be attributed to the improved drug delivery capability of AuNPs and the targeting effect of the cell membrane, as illustrated in Figure 3.

Cell apoptosis appears to be a more sensitive indicator than changes in cell viability for evaluating the therapeutic effects of drugs on tumors. In this study, AnnexinV and 7-AAD staining were employed to analyze cells treated with various drug formulations (Figure 6). Tumor cells treated with DOX for 24 hours exhibited a higher rate of apoptosis compared to the PBS control group, which is consistent with finding from previous researchers. When loaded onto AuNPs, DOX@AuNPs demonstrated an enhanced ability to induce apoptosis. Notably, cells incubated with M@DOX@AuNPs showed the highest apoptosis rate among all groups, including PBS, free DOX, and DOX@AuNPs. These results were consistently observed in both 4T1 and MDA-MB-231 cell lines, indicating that AuNPs can serve as effective drug delivery carriers and that targeting the cell membrane can further enhance the antitumor effect of DOX.

In vivo Anti-Tumor Effect

Due to the excellent intracellular uptake and in vitro tumor cell-killing effect, the anti-tumor efficacy was evaluated using a subcutaneous 4T1 tumor model. For the evaluation of target effects, tumor-bearing mice were administered with DOX, DOX@AuNPs, M@DOX@AuNPs, or PBS as control to assess DOX biodistribution. Eight hours after the first administration, major organs and tumor tissues were collected for fluorescent images. As shown in Figure S6, free DOX primarily accumulated in the liver and lungs. When DOX was loaded onto AuNPs, accumulation in off-target organs was significantly reduced, and increased enrichment was observed in the tumor tissue. Notably, when the nanoparticles were coated with cell membranes, DOX exhibited almost exclusive accumulation at the tumor site. This may be attributed to cell membrane coating, whereby CD47 present on the cell membrane inhibits mononuclear-macrophage phagocytosis, while the cell membrane coating may also enable passive targeting through homologous membrane-mediated mechanisms.

Tumor growth was monitored every two days over a 24-day period starting from the day the tumor model was established. As shown in Figure 7A, DOX, DOX@AuNPs, and M@DOX@AuNPs all demonstrated the ability to inhibit

https://doi.org/10.2147/IJN.S559080

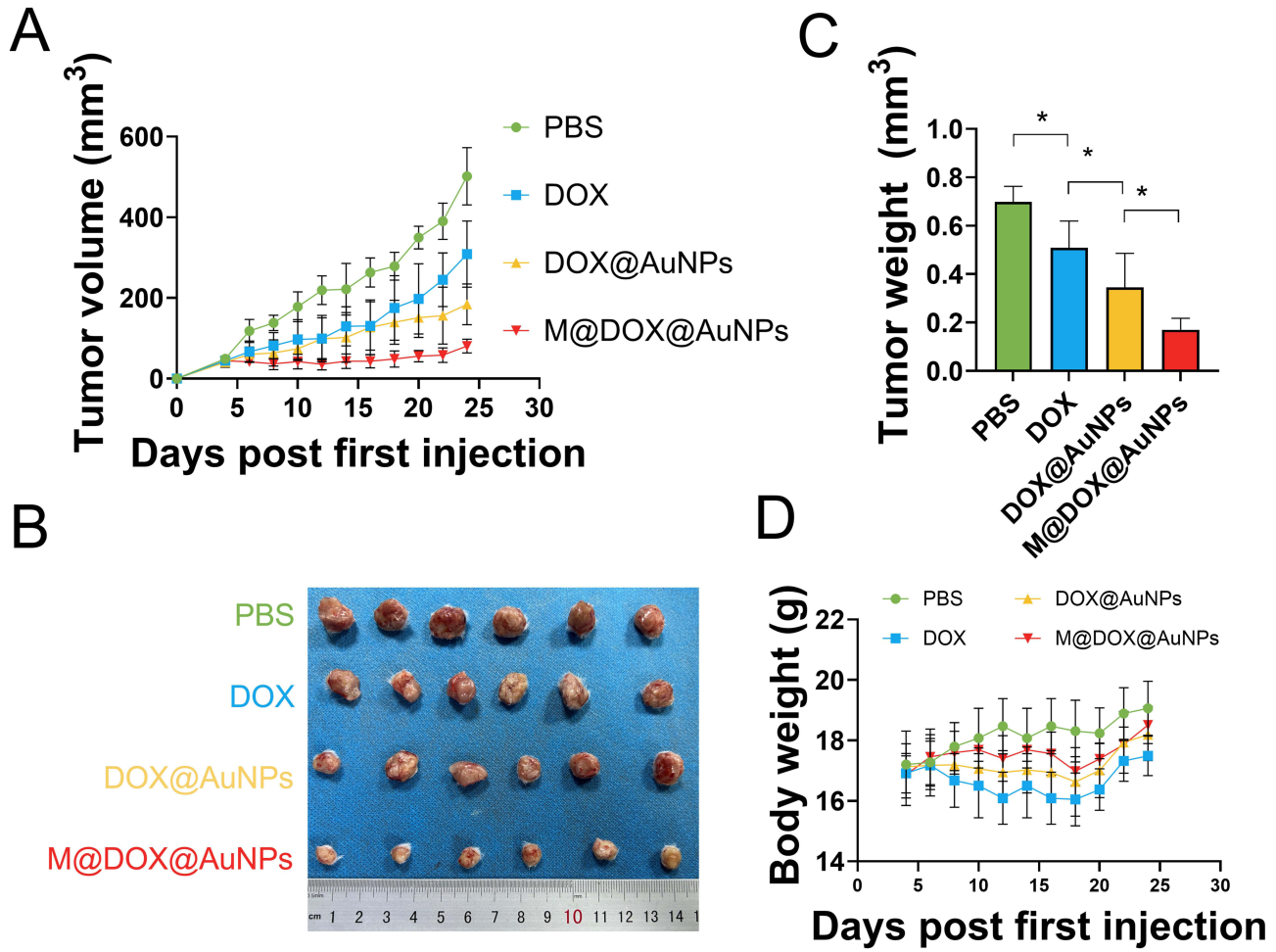

Figure 7 In vivo antitumor efficacy of M@DOX@AuNPs. (A) Tumor growth curves of 4T1 tumor-bearing mice over the course of treatment. (B) Representative photos of excised tumors and (C) quantitative analysis of tumor weights across different treatment groups following 5 times of treatment. (D) body weight changes of 4T tumor-bearing mice over time. Data represent the mean ± SEM from six mice. Statistical significance among groups: *P < 0.05.

tumor growth in the mouse model. Notably, both DOX@AuNPs and M@DOX@AuNPs exhibited enhanced anti-tumor effects, with M@DOX@AuNPs nearly eliminating the tumor. Following the final measurement, the tumors were dissected, photographed and weighted (Figure 7B and C). Consistent with the tumor growth curve, the tumor images and weights both indicated that M@DOX@AuNPs exhibited a superior anti-tumor effect. Body weight monitoring revealed significant fluctuations in the DOX-treated group, which aligns with previous findings (Figure 7D). Interestingly, no significant changes in body weight were observed in M@DOX@AuNPs treated mice. These results clearly demonstrate the potent anti-tumor efficacy of the cell membrane coated drug delivery system.

Biosafety of M@DOX@AuNPs

In the mouse tumor model prior to treatment, the biosafety of the drug delivery system was evaluated by analyzing blood cell counts and assessing the liver and kidney injury markers in the serum, followed by histopathological examination of the major organs via H&E staining. As shown in Figure S7, no significant differences were observed in major blood components, including leukocyte (WBC), red blood cell (RBC), platelet (PLT) and hemoglobin (HB) across the different experimental groups. Additionally, the proportions of immune cell populations – such as monocyte (mono), lymphocyte (lvmph), neutrophils (neut) and eosinophils (eos) – remained largely unchanged. Furthermore, serum levels of liver injury markers (ALT and AST) and the kidney injury marker (Creatinine) were measured (Figure S8), revealing nearly identical results across all four groups.

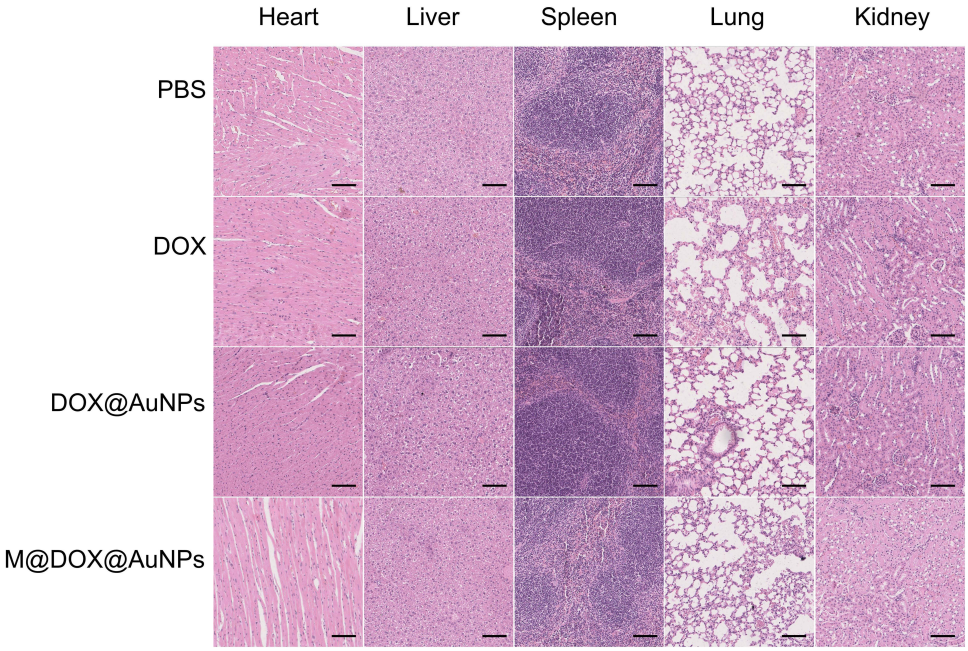

Figure 8 Histological analysis of heart, liver, spleen, lung, and kidney tissues from mice treated with PBS, DOX, DOX@AuNPs, or M@DOX@AuNPs via H&E staining, Scale bar: 100 μm.

Histological analyses were conducted using H&E staining. No tissue damage was observed in the heart, liver, spleen and kidney in any of the treated groups (Figure 8). Mild inflammatory reactions were detected in the lungs of mice treated with DOX; however, these inflammatory responses were significantly reduced in DOX@AuNPs and M@DOX@AuNPs groups. Although, AuNPs may accumulate in organs over the long term, the extent of damage induced by AuNPs is significantly lower than that caused by DOX. Meanwhile, drug loading onto AuNPs significantly reduce their enrichment in lung tissue (Figure S6), thereby further mitigating pulmonary injury. These results indicate that the drug delivery system developed in this study is safe and does not induce organ damage in experimental mice.

Conclusions

In summary, we rationally designed a drug delivery system that specifically targets tumor cells. AuNPs were utilized as drug carriers duo to their excellent drug delivery capability, while cell membrane coating further enhanced M@DOX@AuNPs with high targeting activity in vitro and in vivo. This drug delivery system demonstrated significant anti-tumor effects in 4T1 and MDA-MB-231 tumor cell lines and effectively inhibited tumor growth in a mouse model. Moreover, biosafety was confirmed through in vitro hemolysis tests, biochemical assays, blood cell count analysis from treated mouse, and Histological examination of major organs. Overall, this dual-functional nanomedicine, integrating both targeted delivery and anti-tumor properties, offers a promising and effective strategy for tumor therapy.

Data Sharing Statement

The data will be made available upon reasonable request from the corresponding author.

Author Contributions

All authors made a significant contribution to the work reported, whether that is in the conception, study design, execution, acquisition of data, analysis and interpretation, or in all these areas; took part in drafting, revising or critically reviewing the article; gave final approval of the version to be published; have agreed on the journal to which the article has been submitted; and agree to be accountable for all aspects of the work.

Funding

We sincerely thank the Joint Construction Project of Henan Medical Science and Technology Research and Development Program (LHGJ20230497, LHGJ20250461), Key Research Project Plan for Higher Education Institutions in Henan Province (26B320010) and Xinxiang Key Laboratory of Nanodrug Delivery System Construction and Application for their financial support.

Disclosure

The authors declare that they have no known competing financial interests or personal relationships that could have appeared to influence the work reported in this paper.

References

1. Bray F, Laversanne M, Sung H, et al. Global cancer statistics 2022: GLOBOCAN estimates of incidence and mortality worldwide for 36 cancers in 185 countries. *CA Cancer J Clin*. 2024;74:229–263. doi:10.3322/caac.21834
2. Lim J, Jung HD, Park SY, et al. Genome-scale knockout simulation and clustering analysis of drug-resistant breast cancer cells reveal drug sensitization targets. *Proc Natl Acad Sci U S A*. 2025;122:e2425384122. doi:10.1073/pnas.2425384122
3. Anceschi C, Scavone F, Armanetti P, et al. Antitumoral efficacy of AuNRs-Laden ECFCs in vitro and in vivo: decoding the heat and rays combo treatment in breast cancer and melanoma cells. *Adv Healthc Mater*. 2025;14:2502416. doi:10.1002/adhm.202502416
4. Cai Y, Zhao P, Wu F, et al. Inhibition of NR2F2 restores hormone therapy response to endocrine refractory breast cancers. *Sci Transl Med*. 2025;17:eadk7786. doi:10.1126/scitranslmed.adk7786
5. Xu R, Zhang Y, Liu C, Xu Y, Shao Z, Yu K. Immunotherapy and its racial specificity for breast cancer treatment in Asia: a narrative review. *Lancet Reg Health*. 2025;57:101180. doi:10.1016/j.lanwpc.2024.101180
6. Yu AF, Dang CT, Moskowitz CS, et al. Cardiac safety of reduced cardiotoxicity surveillance during HER2-targeted therapy. *JACC-Cardiooncol*. 2025;7:430–441. doi:10.1016/j.jaccao.2025.05.006
7. Alkan AH, Cansaran-Duman D. Multifaceted interactions between lncRNA-associated ceRNA networks and small molecules in triple-negative breast cancer. *Biomed Pharmacother*. 2025;189:118241. doi:10.1016/j.biopha.2025.118241
8. Srinivasan S, Yee NA, Alečković M, et al. Development of a first-in-class click chemistry–based cancer therapeutic, from preclinical evaluation to a first-in-human dose escalation clinical trial. *Clin Cancer Res*. 2025;OF1–OF16. doi:10.1158/1078-0432.CCR-25-2312
9. Weterings MA, Glanville E, van Eekelen R, Farquhar C. Interventions for fertility preservation in women with cancer undergoing chemotherapy. *Cochrane Database Syst Rev*. 2025;2025:1.
10. Sepúlveda P. Synergistic miRNA combinations mitigate doxorubicin-induced cardiotoxicity. *JACC-Cardiooncol*. 2025;7:411–413. doi:10.1016/j.jaccao.2025.04.002
11. Maleki H, Aiyelabegan HT, Javadi P, et al. Nanotechnology-mediated precision drug delivery strategies for breast cancer treatment. *Biomed Pharmacother*. 2025;188:118224. doi:10.1016/j.biopha.2025.118224
12. Baron R, Haick H. Mobile diagnostic clinics. *ACS Sens*. 2024;9:2777–2792. doi:10.1021/acssensors.4c00636
13. Xu J, Liu W, Fan F, Zhang B, Sun C, Hu Y. Advances in nano-immunotherapy for hematological malignancies. *Exp Hematol Oncol*. 2024;13:57. doi:10.1186/s40164-024-00525-3
14. Gholami A, Mohkam M, Soleimanian S, Sadraeian M, Lauto A. Bacterial nanotechnology as a paradigm in targeted cancer therapeutic delivery and immunotherapy. *Microsyst Nanoeng*. 2024;10:113. doi:10.1038/s41378-024-00743-z
15. He H, Liu L, Morin EE, Liu M, Schwendeman A. Survey of clinical translation of cancer nanomedicines—lessons learned from successes and failures. *Acc Chem Res*. 2019;52:2445–2461. doi:10.1021/acs.accounts.9b00228
16. Soroudi S, Jaafari MR, Arabi L. Lipid nanoparticle (LNP) mediated mRNA delivery in cardiovascular diseases: advances in genome editing and CAR T cell therapy. *J Control Release*. 2024;372:113–140. doi:10.1016/j.jconrel.2024.06.023
17. Guo K, Xiao N, Liu Y, et al. Engineering polymer nanoparticles using cell membrane coating technology and their application in cancer treatments: opportunities and challenges. *Nano Mat Sci*. 2022;4:295–321.
18. Zeng L, Gowda BHJ, Ahmed MG, et al. Advancements in nanoparticle-based treatment approaches for skin cancer therapy. *Mol Cancer*. 2023;22:10.
19. Mohammadpour R, Dobrovolskaia MA, Cheney DL, Greish KF, Ghandehari H. Subchronic and chronic toxicity evaluation of inorganic nanoparticles for delivery applications. *Adv Drug Deliv Rev*. 2019;144:112–132. doi:10.1016/j.addr.2019.07.006
20. Priyadarshi N, Kaushal S, Garg P, et al. Advances in photothermal therapy for cancer and bacterial cells ablation using various nanomaterials. *Adv Colloid Interface Sci*. 2025;342:103541. doi:10.1016/j.cis.2025.103541
21. Singh P, Pandit S, Balusamy SR, et al. Advanced nanomaterials for cancer therapy: gold, silver, and iron oxide nanoparticles in oncological applications. *Adv Healthc Mater*. 2025;14:2403059. doi:10.1002/adhm.202403059
22. Yang M, Wang R, Xie Y, Zhu L, Huang J, Xu W. Applications of DNA functionalized gold nanozymes in biosensing. *Biosens Bioelectron*. 2025;271:116987. doi:10.1016/j.bios.2024.116987
23. Alharbi H. Exploring the frontier of biopolymer-assisted drug delivery: advancements, clinical applications, and future perspectives in cancer nanomedicine. *Drug Design Dev Ther*. 2024;18:2063–2087. doi:10.2147/DDDT.S441325
24. Gavas S, Quazi S, Karpiński TM. Nanoparticles for cancer therapy: current progress and challenges. *Nanoscale Res Lett*. 2021;16:173.
25. An Y, Ji C, Zhang H, et al. Engineered cell membrane coating technologies for biomedical applications: from nanoscale to macroscale. *ACS Nano*. 2025;19:11517–11546. doi:10.1021/acsnano.4c16280
26. Ai X, Wang S, Duan Y, et al. Emerging approaches to functionalizing cell membrane-coated nanoparticles. *Biochemistry*. 2021;60:941–955. doi:10.1021/acs.biochem.0c00343

27. Zhu J, Xie R, Gao R, et al. Multimodal nanoimmunotherapy engages neutrophils to eliminate Staphylococcus aureus infections. *Nat Nanotechnol*. 2024;19:1032–1043. doi:10.1038/s41565-024-01648-8
28. Ding Y, Xu Q, Chai Z, et al. All-stage targeted red blood cell membrane-coated docetaxel nanocrystals for glioma treatment. *J Control Release*. 2024;369:325–334. doi:10.1016/j.jconrel.2024.03.055
29. Kunde SS, Wairkar S. Platelet membrane camouflaged nanoparticles: biomimetic architecture for targeted therapy. *Int J Pharm*. 2021;598:120395. doi:10.1016/j.ijpharm.2021.120395
30. Wang Y, Zhang K, Li T, et al. Macrophage membrane functionalized biomimetic nanoparticles for targeted anti-atherosclerosis applications. *Theranostics*. 2021;11:164–180. doi:10.7150/thno.47841
31. Zhao J, Wang X, Zhang H, et al. Tumor cell membrane biomimetic mesoporous silicon materials in combination with PD-L1 knockout achieved through the CRISPR/Cas9 system for targeted and immunotherapeutic purposes. *Bioconjug Chem*. 2025;36:971–979. doi:10.1021/acs.bioconjchem.5c00001
32. Su N, Villicana C, Barati D, Freeman P, Luo Y, Yang F. Stem cell membrane-coated microribbon scaffolds induce regenerative innate and adaptive immune responses in a critical-size cranial bone defect model. *Adv Mater*. 2023;35:2208781. doi:10.1002/adma.202208781
33. Chen Y, Li Z, Zeng X, Zhang X. Bacteria-based bioactive materials for cancer imaging and therapy. *Adv Drug Deliv Rev*. 2023;193:114696. doi:10.1016/j.addr.2023.114696
34. Fang Z, Zhang M, Kang R, Cui M, Song M, Liu K. A cancer cell membrane coated nanoparticles-based gene delivery system for enhancing cancer therapy. *Int J Pharm*. 2022;629:122415. doi:10.1016/j.ijpharm.2022.122415
35. Pulaski BA, Ostrand-Rosenberg S. Reduction of established spontaneous mammary carcinoma metastases following immunotherapy with major histocompatibility complex class II and B7.1 cell-based tumor vaccines. *Cancer Res*. 1998;58:1486–1493.
36. Brinkley BR, Beall PT, Wible LJ, Mace ML, Turner DS, Cailleau RM. Variations in cell form and cytoskeleton in human breast carcinoma cells in vitro. *Cancer Res*. 1980;40:3118–3129.
37. Zhang Y, Pan D, Zhou Q, et al. An enzyme cascade-based electrochemical immunoassay using a polydopamine–carbon nanotube nanocomposite for signal amplification. *J Mat Chem B*. 2018;6:8180–8187. doi:10.1039/C8TB02659A
38. Fang RH, Hu CJ, Luk BT, et al. Cancer cell membrane-coated nanoparticles for anticancer vaccination and drug delivery. *Nano Lett*. 2014;14:2181–2188. doi:10.1021/nl500618u
39. Zheng F, Tan D, Zheng Y, Chen H, Gao Y. A chitosan-based deep tumor-penetrating nano-photothermal agent for enhanced chemo-photothermal combination therapy. *Mater Today Chem*. 2025;45:102676. doi:10.1016/j.mtchem.2025.102676
40. Cheng LZ, Huang DL, Tang ZR, et al. Pharmacological targeting of Axin2 suppresses cell growth and metastasis in colorectal cancer. *Br J Pharmacol*. 2023;180:3071–3091. doi:10.1111/bph.16193